Trans. JSASS Aerospace Tech. Japan
Vol. 8, pp. 1-7, 2010

Verification of a Charging Potential Measurement Method using a Parallel Plate Electrostatic Analyzer

By Naomi KURAHARA and Mengu CHO

Department of Electrical Engineering, Kyushu Institute of Technology, Kitakyushu, Japan

(Received July 29th, 2009)

The analysis and evaluation of spacecraft charging are important tasks related to spacecraft design. Plasma parameters and charging potential data are needed for charging and discharging predictions. A new type of electrostatic analyzer using two-stage parallel electrodes has been developed to measure the charging potential of a spacecraft over a wide range, from one volt to tens of kilovolts. The spacecraft charging potential is determined by analyzing the energy spectrum shift. A proof-of-concept model of the new electrostatic analyzer was tested in a vacuum chamber filled with Xe plasma. The experimental results agreed very well with the theoretical predictions. The device, made of two parallel plate electrodes, can measure the charging potential by scanning the electrode voltage over only one-tenth of the actual charging potential. The simple structure and low-voltage operation make the device suitable for operation on a small satellite.

Key Words: Spacecraft Charging, Langmuir Probe, Electrostatic Analyzer, Plasma Measurement

Nomenclature

a	:	acceleration between electrodes
m	:	particle mass
d	:	gap length between electrodes
q	:	electrical charge of an incident particle
V_1, V_2	:	voltage difference between bias and GND electrodes at first and second stage
T_{c1}, T_{c2}	:	running time in a cross-wise direction at analyzer first and second stage
T_{L1}, T_{L2}	:	running time in a length-wise direction at analyzer first and second stage
L_1, L_2	:	electrode height of first and second stage
e	:	elementary charge
E	:	particle energy, eV
V_{charge}	:	charging potential
V_{peak}	:	peak position of the current collection for analyzing electrode

1. Introduction

Spacecraft charging has become increasingly important for the stable operation of spacecraft as the spacecraft bus voltage increases. Arcing caused by spacecraft charging sometimes has a fatal effect on spacecraft operational life.[1)] In order to understand spacecraft failure mechanisms, of which the majority are believed to be caused by spacecraft charging,[2)] monitoring the spacecraft charging condition has become an important issue. Although the mechanism of spacecraft charging has been studied for the past 40 years, the on-orbit measurement of spacecraft charging potential has been done only for a limited number of spacecraft.

There are mainly two items for identifying spacecraft charging conditions. One is the spacecraft chassis potential with respect to the surrounding plasma, which we call the "spacecraft charging potential." The other is the spacecraft insulator potential with respect to the spacecraft chassis, which we call the "differential voltage." This paper deals with spacecraft charging potential only. Most of the problems related to spacecraft charging arise when the spacecraft charging potential is negative. When it is positive, the problem is mostly limited to the distortion of scientific measurements. When it is negative, if the differential voltage exceeds a certain value, an electrostatic discharge (ESD) may occur, producing various detrimental effects on spacecraft operation. Therefore, detecting the negative potential of the spacecraft chassis gives the first sign of the anomaly caused by spacecraft charging.

Although the routine and long-term monitoring of spacecraft charging potential is desirable, the measurement device must be adopted to a wide range of charging potential expected in orbit. In a geosynchronous orbit (GEO), it is reported that spacecraft are charged in the range from +10V to -10kV.[3-4)] In a polar earth orbit (PEO), a charging potential below -1kV has been reported.[5)] In low earth orbit (LEO) with a low inclination angle, the charging potential is more or less the negative value of the solar array output voltage.[6)] It is difficult to make a precise measurement for low charging potential (less than ±100V) and high potential (below -100V) using only a single device.[7)]

Regarding the low potential measurement, an electric probe such as a Langmuir probe,[8)] one of the most popular electric probes, is often used for plasma measurement. It was developed in the early 1920s, and since 1960, is often used to measure space plasma and charging potential. A disadvantage of the Langmuir probe is the need of high-voltage biasing to

©2010 The Japan Society for Aeronautical and Space Sciences

cover the large range of charging potential. Another problem is contamination. A contaminated probe surface may give a false result.

Whilst the Langmuir probe is used for low charging potential measurements (-100V < charging potential < 100V), an electrostatic analyzer is suitable for high negative potential measurements (below -100V). Electrostatic analyzers are used to measure the ion or electron energy. In general, an electrostatic analyzer counts a particle (ion or electron) which has certain energy. The energy spectrum can be observed by counting several energies. The highly charged potential is estimated by analyzing the shift in the spectrum. When a spacecraft is negatively charged, ions impacting the spacecraft acquire additional energies by being accelerated inside the negative sheath surrounding the spacecraft. Therefore, the ion energy spectrum shifts to higher energy through the potential energy acquired by the ions.

One problem of energy spectrum measurement with an electrostatic analyzer is that it often measures only discrete bins of fixed energies. For example, the Defense Meteorological Satellite Program (DMSP) satellites, which were developed and operated by the US Air Force, carry an electrostatic analyzer that measures 20 energy bands: ten high-energy bands (0.948, 1.39, 2.04, 3.00, 4.40, 6.46, 9.48, 13.92, 20.44, and 30.00 keV) and ten low-energy bands (30.0, 44.0, 64.6, 94.9, 139.2, 204.4, 300, 440, 646, and 948 eV) are measured. The energy bands measured are determined by the size and bias voltage of the electrostatic analyzer. In general, measuring multiple energy bands requires an increase in the size or number of electrostatic analyzers.

There are several different types of electrostatic analyzers, where the main feature of each type is in the design of the analyzing electrodes. There are parallel plate types,[9-12] a cylinder type,[13] spherical types,[14] and so on. Every electrostatic analyzer uses an electric field generated between the analyzing electrodes to distinguish particle energies. A common problem is that large electrodes for long distances or high biased voltages for large electric fields are required to detect high-energy particles. A parallel plate electrostatic analyzer needs tandem parallel electrodes where each electrode has a length of over 93mm to measure 15eV electrons.[15] Generally, a parallel plate analyzer is used to measure the beam energy spectrum in ground experiments because the analyzer size is fairly large. For on-orbit measurement, cylinder and spherical types are often used. One of the spherical-type electrostatic analyzers requires a diameter of approximately 250mm to detect 200keV energy particles.[16] Another one, which was carried on the CRRES spacecraft, required a diameter of 149mm and a biased voltage of 14.4kV to get an energy measurement range from 1.2 to 427keV.[17] Another problem of electrostatic analyzer measurement is energy resolution. The resolution is often ±10 – 15%.[16, 17] This means a 1keV level measurement contains an error of ±100eV.

Current charging potential measurement has limitations (Table 1). There is no system that measures low and high charging potential using one device. The main issue is their size. The most common size used at present, a diameter of approximately 200mm to measure hundreds of keV of energy, can be carried by a large spacecraft, but not for all types of spacecraft.

Table 1 Charging potential measurement method.

	Advantages	Disadvantages
Langmuir probe	Light, easy, simple system	Contamination, cannot be used in a low-density plasma
Electrostatic analyzer	Can measure a high potential	Heavy, big, complex system

In the present study we try to develop a method to measure high and low spacecraft charging potentials with one device that is small enough to be carried by any type of spacecraft. We have developed a new type of electrostatic analyzer. It uses two sets of parallel plate electrodes to pick up only a fraction of the ions from the wide energy spectrum. The peak of the detected signal shifts depending on the ion drift speed, and from the shift, we can derive the spacecraft charging potential.

In a stable plasma environment, the plasma energy spectrum can be considered to have a peak shape such as Maxwellian or Druyvesteyn distribution. The plasma energy spectrum can be reconstructed by differentiating the current collection characteristic (V-I curve) measured by an electrode in the plasma. The two-stage parallel plate electrostatic analyzer is designed to differentiate the current collection in the plasma using electrodes. The first stage collects particles with energy less than a certain value. The second stage collects a fraction of the remaining particles whose energy is less than a value larger than the threshold of the first stage. Therefore, the second stage picks up a fraction of the particles in the energy spectrum. By making the difference of the maximum energies collected by the first and second stages sufficiently small, we can reconstruct the energy spectrum by varying the energy thresholds of each stage. The advantage of the present electrostatic analyzer over the other types of electrostatic analyzers is its simplicity and compact size, because the primary purpose is focused on measuring the spacecraft charging potential.

This paper presents the results of an experiment carried out in a vacuum chamber to verify the proposed electrostatic analyzer operational principle. The results are also compared with the results of numerical simulation. In the second section of the paper, the operational principle is explained. In the third section, the experiment is presented. In the fourth section, the simulation is presented. In the fifth section, we conclude the paper along with suggestions for future research.

2. Two-Stage Parallel Plate Electrostatic Analyzer

2.1. Analyzer description

Figure 1 shows a schematic picture of the two-stage parallel plate electrodes. Two pairs of parallel plates are placed inside a metallic case. Each pair consists of two plates of the same size. The upper pair is regarded as the first stage, and the lower is regarded as the second stage. The two stages have the same gap distance and are on the same vertical axis. The metallic case is bonded to the spacecraft chassis. The case has

a slit located directly above the electrodes. Energy particles enter the slit and pass through the parallel electrodes toward the bottom. Another electrode (collector) is located at the bottom.

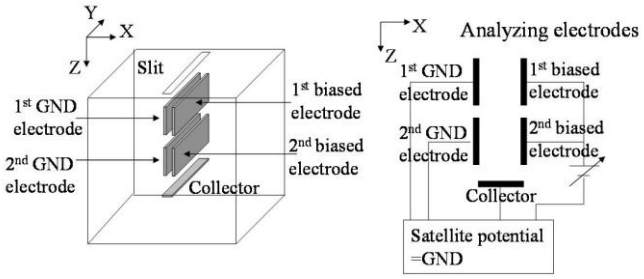

Fig. 1. Schematic picture of two-stage parallel plate electrodes.

At each stage, one electrode is biased to a certain potential with respect to the spacecraft chassis and the other is connected to the case, which is the ground (GND) of the analyzer. The GND has the same potential as the measurement target (=spacecraft chassis). If the spacecraft is charged to -1kV with respect to the surrounding plasma, the GND is also -1kV with respect to the surrounding plasma.

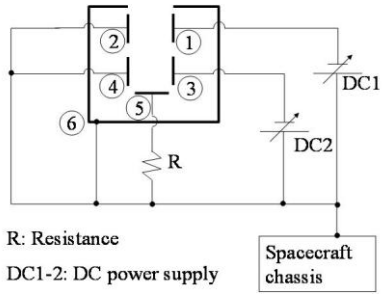

Fig. 2. Test circuit diagram of the measurement system. ①1st-stage biased electrode ②1st-stage GND electrode ③2nd-stage biased electrode ④2nd-stage GND electrode ⑤Collector ⑥Analyzer case

2.2. Operational principle

Most of the particles entering the slit are collected either by the first-stage electrodes, second-stage electrodes, or collector. The most important part of the present measurement is the current collection characteristic of the second-stage electrode. This characteristic corresponds to the plasma energy spectrum.

An electric field is generated between the biased and GND electrodes of each stage. The orbits of ions and electrons are deflected by the electric field. The acceleration is given by

$$a = \frac{qV}{md} \quad . \tag{1}$$

We assume that the initial velocity of a particle parallel to the electric field is zero and the initial position is at the centre of the electrodes. The particle reaches one of the electrodes in the first stage in time, T_{c1}, given by

$$\frac{1}{2} a T_{c1}^{\ 2} = \frac{1}{2} d \tag{2}$$

and

$$T_{c1} = \sqrt{\frac{md^2}{qV_1}} \quad . \tag{3}$$

At the same time, the particle can pass through the first stage in a time, T_{L1}, given by

$$T_{L1} = L_1 \sqrt{\frac{m}{2eE}} \quad , \tag{4}$$

where E is the energy given in electron volts. The particle is collected at the first-stage electrode when the time to pass through the parallel electrodes is shorter than the time to be deflected to the electrodes; that is,

$$T_{c1} < T_{L1} \quad . \tag{5}$$

Substituting Eqs. (3) and (4), a particle collected at the first stage electrode has the following energy:

$$E < E_1 = \frac{q}{2ed^2} V_1 L_1^{\ 2} \quad . \tag{6}$$

Next, consider the second-stage electrode collection. The time to pass through the second stage is given by.

$$T_{L2} = L_2 \sqrt{\frac{m}{2eE}} \quad . \tag{7}$$

The particle entering the second stage has already been accelerated toward the electrode. Therefore, it has the initial velocity parallel to the electric field, $a_1 T_{L1}$, and its initial position is already shifted by $(1/2)a_1 T_{L1}^{\ 2}$, from the center line. For the particle to be collected at the second stage, the following condition has to be satisfied:

$$\frac{1}{2} a_1 T_{L1}^{\ 2} + a_1 T_{L1} T_{L2} + \frac{1}{2} a_2 T_{L2}^{\ 2} > \frac{1}{2} d \quad . \tag{8}$$

Substituting Eqs. (1), (3) and (7), a particle collected at the second-stage electrode has the following energy:

$$E < E_2 = \frac{q}{2ed^2} (V_1 L_1^{\ 2} + 2V_1 L_1 L_2 + V_2 L_2^{\ 2}) \quad . \tag{9}$$

The particles which have energies lower than E_1 given by Eq.(6) have already been collected at the first-stage electrode. The second stage electrode collects only particles which have energies between E_1 and E_2. The energy difference, shown in Eq. (10), is derived by subtracting Eq. (6) from Eq. (9):

$$E_{dif} = \frac{q}{2ed^2} (2V_1 L_1 L_2 + V_2 L_2^{\ 2}) \quad . \tag{10}$$

The current collected at the second stage is integral of the distribution function over the energies between E_1 and E_2.

We take the axis penetrating through the slit in parallel to the parallel plate as the z-axis. For simplicity, we assume a one-dimensional Maxwellian distribution in the z direction, and the z-direction velocity follows that

$$f(v_z) = n\left(\frac{m}{2\pi\kappa T}\right)^{1/2} \exp\left(-\frac{m}{2\kappa T}\left(v - v_o\right)^2\right), \quad (11)$$

where v_o is the drift velocity produced by the acceleration inside the sheath in front of the slit and is written as

$$v_o = \sqrt{\frac{2qV_{chrg}}{m}} \quad . \quad (12)$$

The current collected at the second stage is written in the following integral form:

$$I_2(V_1, V_2) = qA\int_{v_1}^{v_2} v_z f(v_z) dv_z \quad , \quad (13)$$

where the upper and lower limits of the integral are the velocity corresponding to E1 and E2:

and

$$\frac{1}{2}mv_1^{\,2} = E_1$$
$$\frac{1}{2}mv_2^{\,2} = E_2 \quad . \quad (14)$$

Reformulating the data, the current at the second-stage electrode is given by:

$$I_2(V_1, V_2) = qnA\left(\frac{v_o}{\sqrt{\pi}}\int_{t_1}^{t_2}\exp\left(-t^2\right)dt + \frac{1}{2\sqrt{\pi}}\sqrt{\frac{2\kappa T}{m}}\left(\exp\left(-t_1^2\right) - \exp\left(-t_2^2\right)\right)\right), \quad (15)$$

where the variable has been changed to t that is given by

$$t = \frac{v - v_o}{\sqrt{\frac{2\kappa T}{m}}} \quad . \quad (16)$$

We simplify the integral in the bracket using the central value between t_1 and t_2:

$$t_c = \frac{t_1 + t_2}{2} = \left(\frac{2L_1 + L_2}{2\sqrt{2}d}\right)\sqrt{\frac{qV}{\kappa T}} - \sqrt{\frac{qV_c}{\kappa T}} \quad , \quad (17)$$

where the bias voltage of the first and second stages is assumed to be the same (i.e., $V_1=V_2=V$) and Eqs.(6), (9), (14) and (16) are used. Equation 15 is rewritten as:

$$I_2(V) = qnA\left(\frac{v_o}{\sqrt{\pi}}\exp\left(-t_c^{\,2}\right)\left(t_2 - t_1\right) + \frac{1}{2\sqrt{\pi}}\sqrt{\frac{2\kappa T}{m}}\left(\exp\left(-t_1^2\right) - \exp\left(-t_2^2\right)\right)\right), \quad (18)$$

The first term in the bracket is due to the drift velocity and the second term is due to the thermal velocity. As we consider a case where the spacecraft is charged to a potential much larger than the ion temperature, we can neglect the second term. Then, the current is simplified as:

$$I_2(V) \approx qnA\frac{v_o}{\sqrt{2\pi}}\exp\left(-t_c^{\,2}\right)\frac{L_2}{d}\sqrt{\frac{qV}{\kappa T}} \quad . \quad (19)$$

The variable t_c changes from minus to positive. The current has a peak when $t_c=0$. Therefore, from Eq.(17), the voltage V_{peak} which gives the current peak satisfies the following equation:

$$V_c = \frac{\left(2L_1 + L_2\right)^2}{8d^2}V_{peak} \quad . \quad (20)$$

Therefore, from the peak position of the collected current, we can deduce the charging potential.

3. Verification Test

3.1. Model

An experimental model of the two-stage parallel plate electrostatic analyzer was built and tested in a plasma chamber. Figure 3 shows a photograph of the model. The volume of the experimental model is only 125cm^3. It has the electrodes only and does not include any electronics, although there is plenty of space inside the box. There is a 2mm-wide slit on the top. The analyzing electrodes are located just under the slit. The schematic plan of the analyzing electrodes is shown in Fig. 4. A total of four electrodes are fixed on the two placing plates. Each electrode is insulated from the placing plate by boron nitride (BN). The gap between the electrodes, *d*, is 1.7mm. The vertical length of the first- and second-stage electrodes is 5mm for all electrodes (i.e., $L_1=L_2=5mm$). The distance between the first and second stages is 1.5mm. Each length has an error of ±0.2mm.

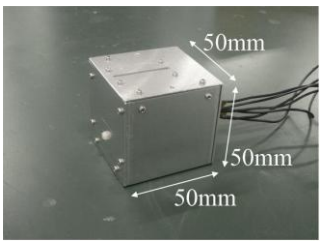

Fig. 3. Appearance of the verification model of the electrostatic analyzer, 50×50×50mm size. There is a 2mm-wide slit on the top.

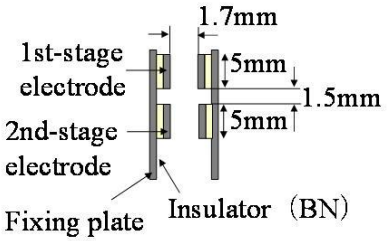

Fig. 4. Schematic plan of the analyzing electrodes. Electrodes are placed on anchoring plates with an insulator between the electrode and the plate.

The experimental model was placed in a plasma chamber. The chamber is a cylinder of 1m in diameter and 1.2m in length, and is filled with Xenon plasma. The typical plasma parameters during the test are listed in Table 2. The tests were performed at different charging potentials by biasing the analyzer external frame from -10V to -500V with respect to the chamber wall.

Table 2 Plasma parameters for testing environment.

Density	$5(\pm 2) \times 10^{12}$ m^{-3}
Temperature	1eV (±0.5eV)
Debye length	2.5mm (±1mm)
Potential	3V (±5V)

3.2. Test results

Figure 5 shows the voltage-current characteristics of the analyzing electrodes when the charging potential is -150V. We can confirm that the current waveform of the second-stage electrode has a peak. Figs. 6 and 7 show how the peak position shifts at the second biased and GND electrodes. The peak position of the GND electrode shifts in the positive direction and the peak position of the biased electrode shifts in the negative direction. The current-voltage characteristics of the second-stage electrode tend to become flat near the peak value as the charging potential becomes more negative. This causes uncertainty, from which the charging potential is derived.

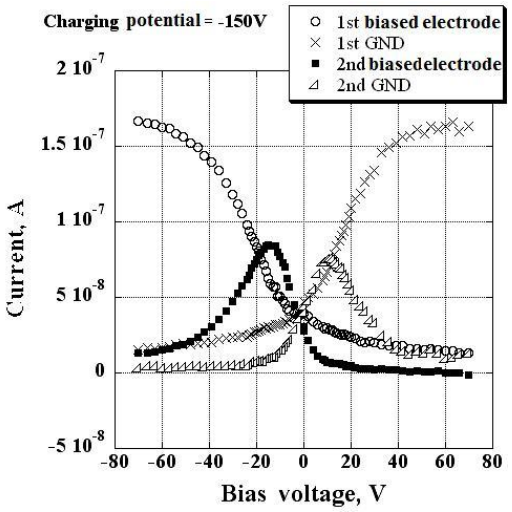

Fig. 5. Voltage-current characteristics of biased and GND electrodes at the first and second stages. The charging potential is -150V.

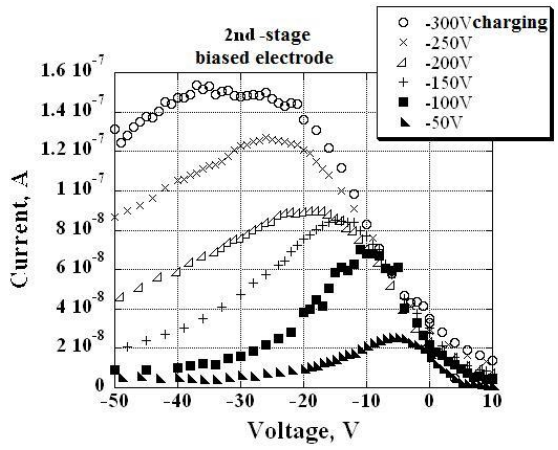

Fig. 6. Peak position shift at the second biased electrode.

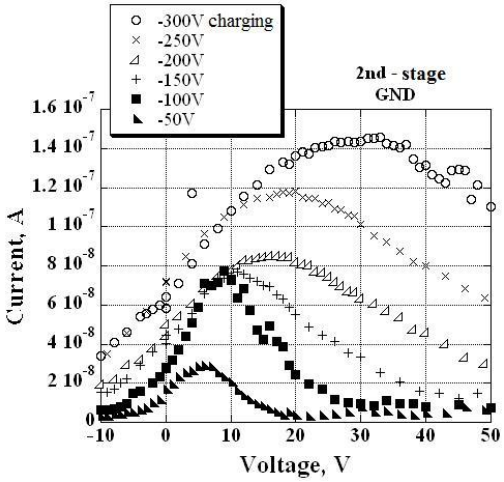

Fig. 7. Peak position shift at the second GND electrode.

3.3. Charging potential

The amount of peak position shift with the charging potential is plotted in Figs. 8 and 9. We define the peak area as the bias voltages that give more than 95% of the maximum current. The peak position is the mean value of the peak area, and the error bar corresponds to the upper and lower bounds of the peak area.

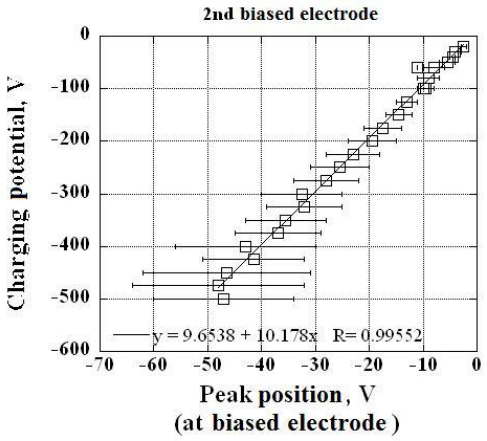

Fig. 8. Peak position vs. charging potential at the second biased electrode.

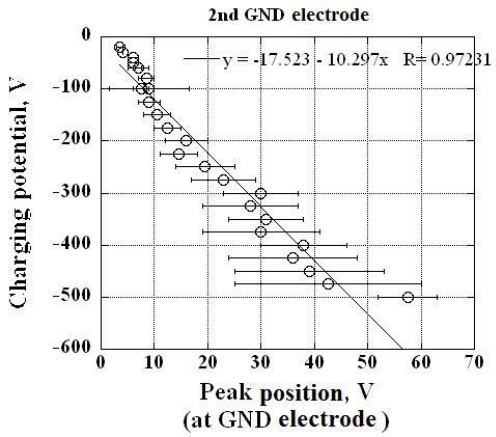

Fig. 9. Peak position vs. charging potential at the second GND electrode.

The relationship between the bias voltage of the peak position, V_{peak}, at the second bias electrode and the charging potential V_c is approximated by

$$V_c = 10.2V_{peak} + 9.7 \quad . \tag{21}$$

The relationship of the second GND electrode is approximated by

$$V_c = -10.3V_{peak} - 17.5 \quad . \tag{22}$$

The theory of current collection for electrodes was discussed in section 2.3. When parameters of the electrostatic analyzer from the validation model are applied to Eqs. (6) and (9), the energy range of the ions collected by the second electrode is given by

$$4.3V < E < 17.3V \tag{23}$$

Eqations (6) and (9) and experimental results, Eqs. (22) and (23), are plotted in Fig. 10. As it is shown in Fig. 10, experiment results take almost the average value between E_1 and E_2.

As shown in Figs. 6 and 7, the peak becomes relatively flat as the charging potential increases. The energy range collected by the second electrode is given by Eq. (10). By dividing the energy range by the center value between E_1 and E_2, we obtain

$$\frac{\Delta E}{E} \approx \frac{E_{diff}}{\frac{E_1+E_2}{2}} == \frac{2L_1L_2 + {L_2}^2}{2{L_1}^2 + L_1L_2 + {L_2}^2} = \frac{\frac{L_2}{L_1} + \frac{{L_2}^2}{2{L_1}^2}}{2 + \frac{L_2}{2L_1} + \frac{{L_2}^2}{2{L_1}^2}}, \tag{24}$$

where $V_1=V_2$ is assumed. From this equation, making the second-stage electrode length L_2 much shorter than the first-stage electrode length makes the peak narrower.

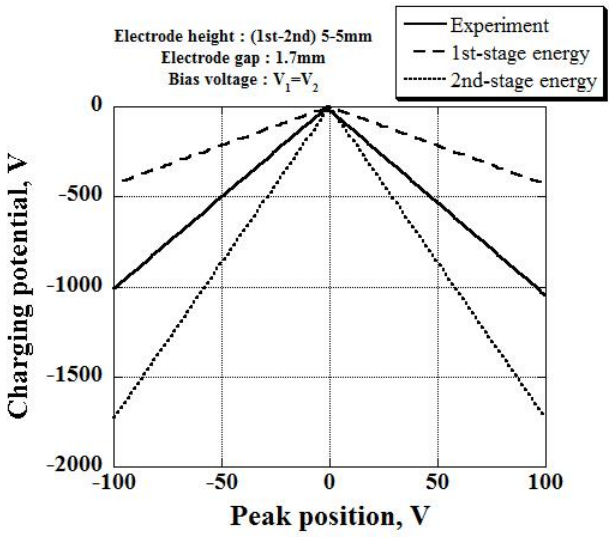

Fig. 10. Comparison of charging potential equations.

As we substitute the values of L_1, L_2 and d into the theoretical prediction Eq. (20), we obtain the following formula:

$$V_c = 9.73V_{peak} \quad . \tag{25}$$

Considering the assumptions made to derive Eq. (20), the agreement between the theory and the experiment is very good.

4. Simulation

Numerical simulation was carried out, including the effect of two-dimensional Maxwellian distribution. The ions are assumed to enter the parallel electrode uniformly over the width d. We divide the distribution function into 100 bins of the velocities in x and z directions, where the x-axis is parallel to the applied electric field and the z-axis is parallel to the electrode penetrating through the slit. The potential energy gained in the sheath is given as the drift velocity in the z-direction. We judge which electrode a particle of a given set of the initial velocities and the initial position hits for a given bias voltage V. In total, 1,000,000 cases of combinations of initial velocities and positions are observed.

Figure 11 shows the results of the case where the particle is accelerated to 150eV before entering the slit. Parameters for analyzing electrode size are same as the experiment. In Fig. 12, we plot the experimental and simulation results. The experimental and simulation results agree very well, verifying the operational principle.

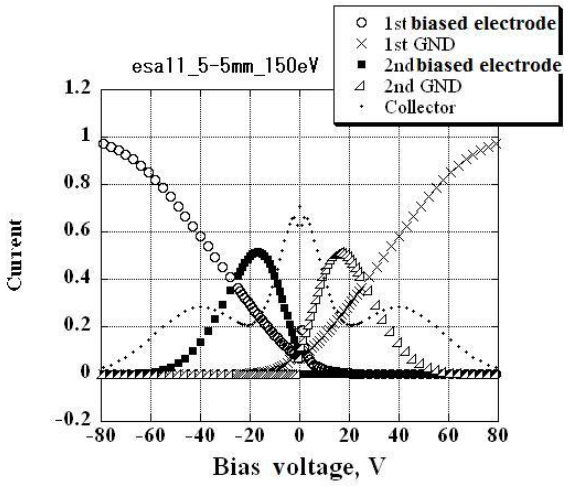

Fig. 11. Simulation result of 150eV particle energy. Electrode heights of each stage are both 5mm.

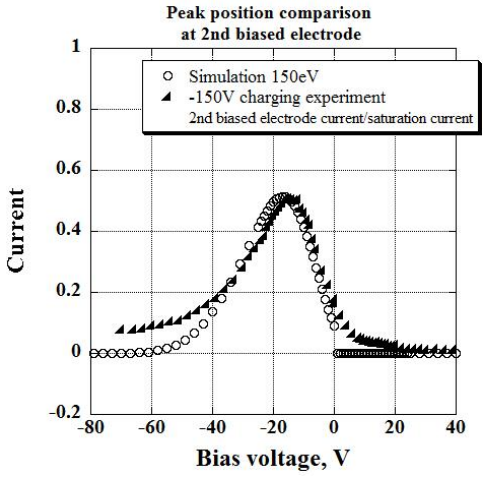

Fig. 12. Comparison of current collection at second biased electrode. Experimental results are normalized by the saturation current.

At the second-stage electrodes, the voltage-current characteristic shows a peak very similar to the experimental results. Peak positions shift as the charging potential changes. The charging potential-peak position characteristic is derived from the numerical simulation and compared with that from the experimental results. The peak position can be approximated by the following equation:

$$V_{charge} = 9.31 V_{peak} + 6.3 \quad . \qquad (26)$$

The number is fairly close to the experimental and theoretical values.

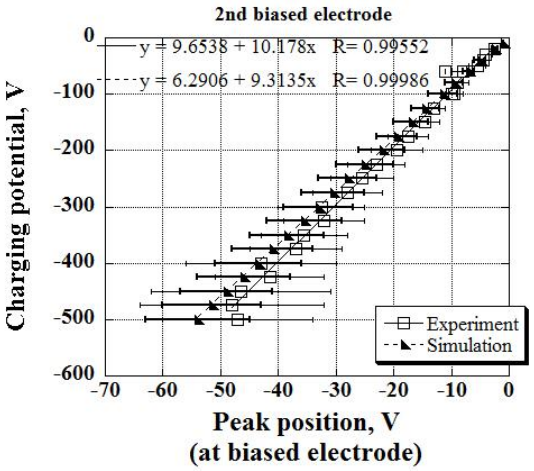

Fig. 13. Comparison of charging potential-peak position characteristics.

5. Conclusion and Future Research

To measure a wide range of spacecraft charging potentials with a simple device, a two-stage parallel plate electrostatic analyzer has been developed. A theoretical model of the current collection by the analyzing electrodes and its relationship to determing the charging potential have been discussed. A verification test was carried out in a vacuum chamber filled with Xenon plasma. The experimental results proved that the two-stage parallel plate electrostatic analyzer was capable of measuring the spacecraft charging potential. The experimental results, theoretical prediction and numerical simulation agreed with each other. The main advantage of the two-stage parallel plate electrostatic analyzer is its simple structure and the use of low bias voltage to measure a high charging potential. The required bias voltage of the measurement was one-tenth of the charging potential for the present verification model.

In the present verification model, the peak of the collected current became flatter as the charging potential roes. To avoid uncertainty, making the second-stage electrode length much shorter than the first-stage electrode is a solution. That solution, however, makes the collected current smaller, which may make the measurement difficult, especially for a low-density plasma. The use of a current amplifier and increasing the length of the slit will provide a solution. In the near future, the improvements will be incorporated into a prototype, which will be further tested.

References

1) Hoeber, C. F., Robertson, E. A., Katz, I., Davis, V. A. and Snyder, D. B.: Solar Array Augmented Electrostatic Discharge in GEO, Proceedings of the 17th International Communications Satellite Systems Conference and Exhibit, 1998, AIAA-1998-1401.
2) Koons, H. C., Mazur, J. E., Selenick, R. S., Blake, J. B., Fennell, J. F., Roeder, J. L. and Anderson, P. C.: The Impact of the Space Environment on Space Systems, Proceedings of the 6th Spacecraft Charging Technology Conference, 2000, AFRL-VS-TR-20001578.
3) Deforest, S. E.: Spacecraft Charging at Synchronous Orbit, *J. Geophys. Res.*, **77** (1972), pp. 651-659.
4) Deforest, S. E.: Electrostatic Potentials Developed by ATS-5, in *Photon and Particle Interactions with Surfaces in Space*, D. Reidel, Hingham, Mass., 1973, pp. 263-276.
5) Wahlund, J. E., Wedin, L. J., Carrozi, T., Eriksson, A. I., Holback, B., Andersson, L. and Laakso, H.: Analysis of Freja Charging Events: Charging Events Identification and Case Study, ESA Technical Note, SPEE-WP110-TN, 1999.
6) Sasaki, S.: Plasma Effects Driven by Electromotive Force of Spacecraft Solar Array, *Geophysical Research Lett.*, **26** (1999), pp. 1809-1812.
7) Garrett, H. B.: The Charging of Spacecraft Surfaces, *Reviews of Geophysics and Space Physics*, **19** (1981), pp. 577-616.
8) Langmuir, I. and Blodgett, K. B.: Currents Limited by Space Charge between Concentric Spheres, *Phys. Rev.*, **24** (1924), pp. 49-59.
9) Green, T. S. and Proca, G. A.: A Parallel Plate Electrostatic Spectrograph, *Rev. Sci. Instrum.*, **41** (1970), pp. 1409-1414.
10) Proca, G. A. and Rudinger, C.: Minimization of Fringing Field Effects in the Parallel Plate Electrostatic Spectrograph, *Rev. Sci. Instrum.*, **44** (1973), pp. 1381-1386.
11) Calabrese, D., Yenen, O., Wiese, L. M. and Jaecks, D. H.: Two-stage Parallel-plate Energy Analyzer for Simultaneous Detection of Positive, Negative, and Neutral Particles, *Rev. Sci. Instrum.*, **65** (1994), pp. 116-122.
12) Hamada, Y., Fujisawa, A., Iguchi, H., Nishizawa, A. and Kawasumi, Y.: A Tandem Parallel Plate Analyzer, *Rev. Sci. Instrum.*, **68** (1997), pp. 2020-2022.
13) Hughes, A. L. and McMillen, J. H.: Re-focussing of Electron Paths in a Radial Electrostatic Field, *Phys. Rev.*, **34** (1929), pp. 291-295.
14) Paolini, F. R. and Theodoridis, G. C.: Charged Particle Transmission through Spherical Plate Electrostatic Analyzers, *Rev. Sci. Instrum.*, **38** (1967), pp. 579-588.
15) Kövér, Á. and Laricchia, G.: A Parallel-plate Analyzer with Time Focusing, *Meas. Sci. Technol.*, **12** (2001), pp. 1875-1880.
16) Kasahara, S., Asamura, K., Ogasawara, K., Mitani, T., Hirahara, M., Takashima, T., Saito, Y. and Mukai, T.: Medium Energy Ion Mass Spectrometer Capable of Measurements of Three-Dimensional Distribution Functions in Space, *IEEE Transactions on Plasma Science*, **36**, 3 (2008), pp. 841-847.
17) Wilken, B. and Weiβ, W.: Magnetospheric Ion Composition Spectrometer Onboard the CRRES Spacecraft, *Journal of Spacecraft and Rockets*, **29** (1992), pp. 585-591.